Food Chemistry 451 (2024) 139427

Contents lists available at ScienceDirect

Food Chemistry

journal homepage: www.elsevier.com/locate/foodchem

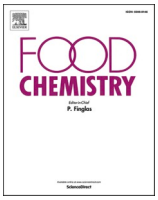

Tuning the planarity of molecularly imprinted covalent organic frameworks for selective extraction of ochratoxin A in alcohol samples

Hao-Ze Li [a,b,c], Hai-Long Qian [a,b,c], Shu-Ting Xu [a,b,c], Cheng Yang [a,b,c], Xiu-Ping Yan [a,b,c,d,*]

[a] State Key Laboratory of Food Science and Resources, Jiangnan University, Wuxi 214122, China
[b] International Joint Laboratory on Food Safety, Jiangnan University, Wuxi 214122, China
[c] Institute of Analytical Food Safety, School of Food Science and Technology, Jiangnan University, Wuxi 214122, China
[d] Key Laboratory of Synthetic and Biological Colloids, Ministry of Education, Jiangnan University, Wuxi 214122, China

ARTICLE INFO

Keywords:
Molecularly imprinted polymers
Covalent organic frameworks
Ochratoxin A
Planarity modulation
Solid phase extraction

ABSTRACT

Here, we report a monomer planarity modulation strategy for room-temperature constructing molecularly imprinted-covalent organic frameworks (MI-COFs) for selective extraction of ochratoxin A (OTA). 2,4,6-triformylphloroglucinol (Tp) was used as basic building block, while three amino monomers with different planarity were employed as modulators to explore the effect of planarity on the selectivity of MI-COFs. The MI-TpTapa constructed from Tp and the lowest planarity of monomer Tapa gave the highest selectivity for OTA, and was further used as the adsorbent for dispersed-solid phase extraction (DSPE) of OTA in alcohol samples. Coupling MI-TpTapa based DSPE with high-performance liquid chromatography allowed the matrix-effect free determination of OTA in alcohol samples with the limit of detection of 0.023 μg kg^{-1} and the recoveries of 91.4–97.6%. The relative standard deviation (RSD, $n = 6$) of intra and inter day was <3.2%. This work provides a new way to construct MI-COFs for selective extraction of hazardous targets.

1. Introduction

Ochratoxin A (OTA), a toxic secondary metabolite produced by *Aspergillus* and *Penicillium* fungi, can survive even after the host fungus is eliminated due to its stability (Samuel et al., 2021). Consequently, OTA is often detected in foodstuffs such as cereals, beer and grape products. The exposure of OTA may cause teratogenicity, immunotoxicity, nephrotoxicity, hepatotoxicity and carcinogenesis (Li, Ma, Ma, Zhang, & Li, 2021a; Su et al., 2022). Thus, OTA has been classified to Group 2B carcinogen by World Health Organization (WHO) (Bui-Klimke & Wu, 2015). The European Commission and Chinese food safety standards (GB 2761–2017) set the maximum residue limit (MRL, 2 μg kg^{-1}) for OTA in alcohol (Zhang et al., 2024). Therefore, selective determination of OTA in foodstuff is of great significance for safeguard food safety and public health.

Various effective analytical methods for the determination of OTA, including immunological methods (Fadlalla et al., 2020), thin-layer chromatography (Pittet & Royer, 2002), liquid chromatography (Li, Ma, Ma, Zhang, & Li, 2021b) and biosensors (Meira et al., 2023), have been developed. No matter what analytical technique is used, sample pretreatment is an essential step before quantitative analysis and directly affects the accuracy and precision of quantitative analysis (Zhang et al., 2019). Compared to other pretreatment methods such as liquid-liquid extraction (Elik, Ablak, Haq, Boczkaj, & Altunay, 2023) and immunoaffinity column extraction (Kabak, 2012), dispersive solid-phase extraction (DSPE) is simple, reusable and less solvent consumption (Huertas-Pérez, Arroyo-Manzanares, García-Campaña, & Gámiz-Gracia, 2017). DSPE adsorbents such as graphene oxide (Cui et al., 2020), metal-organic frameworks (Mohebbi, Nemati, Farajzadeh, Afshar Mogaddam, & Lotfipour, 2022) and zirconia (Du et al., 2018) have been used in the extraction of OTA. However, these adsorbents lack sufficient selectivity for OTA in complex matrices. Therefore, the development of highly selective DSPE adsorbents for OTA determination is greatly imperative.

Covalent organic frameworks (COFs) are porous crystalline materials created by linking organic building (Liu et al., 2021; Ma et al., 2019). COFs are attractive adsorbents for sample pretreatment due to their unique properties such as large surface area, ordered channel and predesigned structure (Chen et al., 2019; Jagirani, Gumus, & Soylak, 2023; Jagirani & Soylak, 2020; Lohse & Bein, 2018; Xin et al., 2020). Some studies on the use of COFs as DSPE adsorbents for the extraction of mycotoxins have been reported (Li et al., 2022; Li et al., 2022; Wei et al.,

* Corresponding author at: State Key Laboratory of Food Science and Resources, Jiangnan University, Wuxi 214122, China.
E-mail address: xpyan@jiangnan.edu.cn (X.-P. Yan).

https://doi.org/10.1016/j.foodchem.2024.139427
Received 7 March 2024; Received in revised form 16 April 2024; Accepted 18 April 2024
Available online 23 April 2024

2023). However, the COFs in these studies cannot meet the requirement for the selective extraction of mycotoxins. To enhance the selectivity of COFs for target, integrating molecular imprinting into COFs is a promising way for the preparation of molecule imprinted COFs (MI-COFs) for the selective extraction of hazardous compounds. There are two main approaches to the synthesis of MI-COFs. One is to load traditional molecularly imprinted polymers (MIPs) on the surface of COFs (Han, Leng, Teng, Ding, & Yao, 2022; Li, Lv, Yang, et al., 2022; Zhao et al., 2023). The other is one-pot method polymerization via monomers and template (Ji, Sun, Geng, Liu, & Wang, 2018; Li et al., 2019; Zhao et al., 2020). However, how to make a reasonable choice of monomers to construct MI-COFs remains challenging.

The monomer with large π-surface area in two-dimensional COFs is conducive to the interlayer π-π stacking (Halder et al., 2016; Martinez-Abadia & Mateo-Alonso, 2020). Several studies on modulating the planarity of monomer to enhance the interlayer interaction of COFs have been reported. For instance, Lotsch's group (Vyas et al., 2015) reported a series COFs (N_x–COF, x = 0–3) with the varying number of nitrogen atoms in central aryl ring for hydrogen generation. The results demonstrated the N_3–COF gave the highest hydrogen production due to the high crystallinity resulting from the planarity of the triazine. Du's group (Jiang et al., 2022) proposed a strategy for enhancing the interlayer interactions of COFs via importing planar triazine units into the center of monomers. The prepared TPT-COF gave about 10 times proton conductivity than non-planar COFs. Yan's group (Da, Yang, Qian, & Yan, 2020) reported a knot-linker planarity control strategy to prepare three ionic COFs (iCOFs) for the removal of 2,4-dichlorophenol. The obtained highly crystalline TFPT–TG_{Cl}–iCOF with planar units gave the largest adsorption capacity and ultrafast kinetics. The above studies reveal that the increase in the planarity of monomer can enhance the interlayer π–π stacking interaction and further improve the crystallinity and the performance of COFs in various applications. However, whether the enhancement of interlayer interaction will promote the high selectivity of MI-COFs for the extraction of analytes is still unclear.

In this work, we propose a monomer planarity modulation strategy for room-temperature constructing MI-COFs for the selective extraction of OTA. Fmoc-D-phenylalanine (Fmoc-D-Phe) was selected as pseudo template for OTA based on space size and theoretical calculation. 2,4,6-triformylphloroglucinol (Tp) was used as basic building block. Three amino monomers with different planarity, including tris (4-aminophenyl) amine (Tapa), 1,3,5-tris (4-aminophenyl) benzene (Tapb) and 4,4′,4″-(1,3,5-triazine-2,4,6-triyl) trianiline (Tz) were selected as modulators to explore the effect of planarity on the selectivity of MI-COFs. The lowest planarity of Tapa monomer gave the best selectivity of MI-COF (called TpTapa) for OTA. The prepared MI-TpTapa was further employed as DSPE adsorbent for the selective extraction of OTA in alcohol samples before HPLC determination of OTA.

2. Experimental

2.1. Chemicals

All reagents used are analytical grade unless otherwise specified. Tp, Tapa, Tapb and Tz were gotten from Jilin Yanshen Technology Co., Ltd. (Jilin, China). 1-Butyl-3-methylimidazolium (BMIm) ion liquids (ILs), including bis(trifluoromethylsulfonyl)imide ([BMIm][NTf_2]), hydrogen sulfate ([BMIm][HSO_4]), trifluoromethanesulfonate ([BMIm][OTf]), tetrafluoroborate ([BMIm][BF_4]) and acetate ([BMIm][Ac]) were obtained from Beijing Innochem Technology Co., Ltd. (Beijing, China). The standard solutions of OTA, zearalenone (ZEN), deoxynivalenol (DON) and aflatoxin B1 (AFB1) were gotten from Anpel Laboratory Technologies Co., Ltd. (Shanghai, China). Fmoc-D-Phe, phenylalanine (Phe), *N*-benzoyl-L-tyrosine ethyl ester (BTEE) and naringenin (Nar) came from Shanghai Aladdin Biochemical Technology Co., Ltd. (Shanghai, China). *N,N*-Dimethylformamide (DMF), acetonitrile (ACN), methanol (MeOH), tetrahydrofuran (THF), acetic acid (HAc), formic acid (FA), sodium hydroxide (NaOH) and hydrochloric acid (HCl) were purchased from Sinopharm Chemical Reagent Co., Ltd. (Shanghai, China). HPLC-grade acetonitrile (ACN) and methanol (MeOH) were purchased from Thermo Fisher Scientific (Shanghai, China). Ultrapure water was given by Wahaha Foods Co., Ltd. (Hangzhou, China).

2.2. Instrumentation

The determination of OTA was performed on e2695 HPLC-2475 FLD (Waters, U.S.A.) equipped with XBridege® C18 column (5 μm, 4.6 mm × 250 mm) at 30 °C. The flow rate of mobile phase ACN/2% HAc solution (50:50, *v*/v) was 1 mL min^{-1}. The sample volume injected was set to 20 μL. The excitation and emission wavelength for the detector were set at 333 nm and 447 nm, respectively.

Other instruments for materials characterization were described in Supplementary Material.

2.3. Synthesis of MI-COFs and NI-COFs

Tp (0.1 mmol, 21 mg) and 0.1 mmol of amino monomers (Tapa, Tapb or Tz) were dispersed in 200 μL of [BMIm][NTf_2]. Then, 50 μL of DMF (contained 12.9 mg of Fmoc-D-Phe) was added. After a 5-min sonification, the mixture was left at room temperature for 12 h. The resulting MI-COF was collected and washed sequentially with DMF, THF, MeOH/HAc (v/v, 9:1) and MeOH until no template was detected by UV–visible spectrophotometry. Finally, the product was dried at 60 °C under vacuum overnight. The NI-COF was prepared in parallel to the MI-COF but in the absence of the pseudo template.

2.4. Adsorption experiments

Adsorption studies were carried on a shaker with the rotate speed 180 rpm at room temperature. The concentration of Fmoc-D-Phe was measured by UV–visible spectrophotometry at 264 nm. For adsorption kinetics study, 1 mg of MI-COFs or NI-COFs (TpTapa, TpTapb and TpTz) was dispersed in 4 mL of Fmoc-D-Phe with the initial concentration of 20 mg L^{-1} (pH 6.5). After adsorption for a certain time (2–60 min), the mixtures were filtered with 0.22 μm filter. To get adsorption isotherms, MI-COFs or NI-COFs (1 mg) was dispersed in 4 mL of Fmoc-D-Phe in the initial concentration range from 40 to 200 mg L^{-1} (pH 6.5). After adsorption for 1 h, the mixtures were filtered with 0.22 μm filter.

To test the selectivity of MI-COFs for the adsorption of OTA, three other mycotoxins, including AFB1, ZEN and DON were selected for comparison. 1 mg of MI-COF or NI-COF was added into 4 mL of 10 mg L^{-1} each mycotoxin solutions. After 1 h of shaking at room temperature, the mixture was filtered with 0.22 μm filter membrane and the concentration of mycotoxin was measured by HPLC.

The adsorption capacity (q, mg g^{-1}) and imprinting factor (IF) were calculated according to Eq. 1 and 2, respectively:

$$q = \frac{C_0 - C_t}{m} V \tag{1}$$

$$IF = \frac{q_{MI-COF}}{q_{NI-COF}} \tag{2}$$

where C_0 (mg L^{-1}) and C_t (mg L^{-1}) stand for the initial and final concentration of adsorbate, respectively. m (mg) represents adsorbent mass, and V (mL) is solution volume. $q_{MI\text{-}COF}$ and $q_{NI\text{-}COF}$ are the adsorption capacity for MI-COF and NI-COF, respectively.

2.5. Sample preparation and DSPE procedure

Beer, soju and red wine were purchased from a local supermarket. The wine sample was ultrasonically treated for 30 min before use. 4 mg of MI-TpTapa was added into 10 g of wine sample with sonication, then the mixture was shaken on a shaker at 180 rpm for 2 min. The MI-

TpTapa was collected by centrifugation at 10000 rpm for 10 min, then eluted with 1 mL of FA/ACN (6:4, *v*/v) for 2 min. The eluent was filtered with 0.22 μm filter membrane and the concentration of OTA was measured by HPLC.

3. Results and discussion

3.1. Design and synthesis of MI-COFs

Fig. 1a illustrates the scheme for the synthesis of MI-COFs. Tp was selected as a basic building block to provide hydrogen bond and π-π interaction with OTAs. The linkage of Tp-based COFs is more stable due to the irreversible proton tautomerism of enol−imine (-OH) form (Kandambeth et al., 2012). Three triamine linkers with different planarity were used as modulators to adjust the interlayer interaction of MI-COFs. The dihedral angle of triamine linkers were calculated to 0.0°, 9.3° and 27.3° for Tz, Tapb and Tapa, respectively (Fig. 1b-d).

Considering the high toxicity and high price of OTA, four OTA structure analogues including Phe, Nar, BTEE and Fmoc-D-Phe were used as pseudo templates to evaluate the effect of template on imprinting effect. The structure and space size of pseudo templates are presented in Fig. S1. Fmoc-D-Phe and OTA contain the structure of Phe. Furthermore, the pk_a of Fmoc-D-Phe (3.77) and OTA (3.29) is close. Molecular docking gave the lowest binding energy of OTA (−6.3 kcal mol^{-1}), Nar (−5.5 kcal mol^{-1}), BTEE (−5.1 kcal mol^{-1}), Phe (−4.1 kcal mol^{-1}) and Fmoc-D-Phe (−6.9 kcal mol^{-1}) with TpTapa (Fig. S2). The lowest binding energy of Fmoc-D-Phe-TpTapa is closest to that of OTA-TpTapa. The π-π and hydrogen bond (N-H…O=C) interactions were observed in the lowest binding energy configuration of OTA with TpTapa, while hydrogen bond interaction was not seen in the lowest binding energy configuration of pseudo templates with TpTapa. Notably, among the possible Fmoc-D-Phe-TpTapa binding configurations, a configuration containing hydrogen bonding NH…O=C the binding energy is also −6.3 kcal mol^{-1} was found to be similar to the lowest binding energy configuration of OTA-TpTapa (Fig. S2e). The above theoretical calculation results preliminarily show that Fmoc-D-Phe is the optimal pseudo template for OTA. Adsorption experiments showed that Fmoc-D-Phe as the pseudo template gave the largest adsorption capacity of MI-TpTapa for OTA (Fig. 2a). The added amount of Fmoc-D-Phe was further investigated. The ratio of monomer/template = 3:1 gave the best imprinting effect, thus used for further experiment (Fig. 2b).

We further investigated the effect of triamine monomers on the imprinting effect of MI-COFs. The value of IF increased with the decrease in the planarity of triamine monomers (Fig. 2c). The result indicates that the non-planar monomer Tapa is more conducive to the formation of

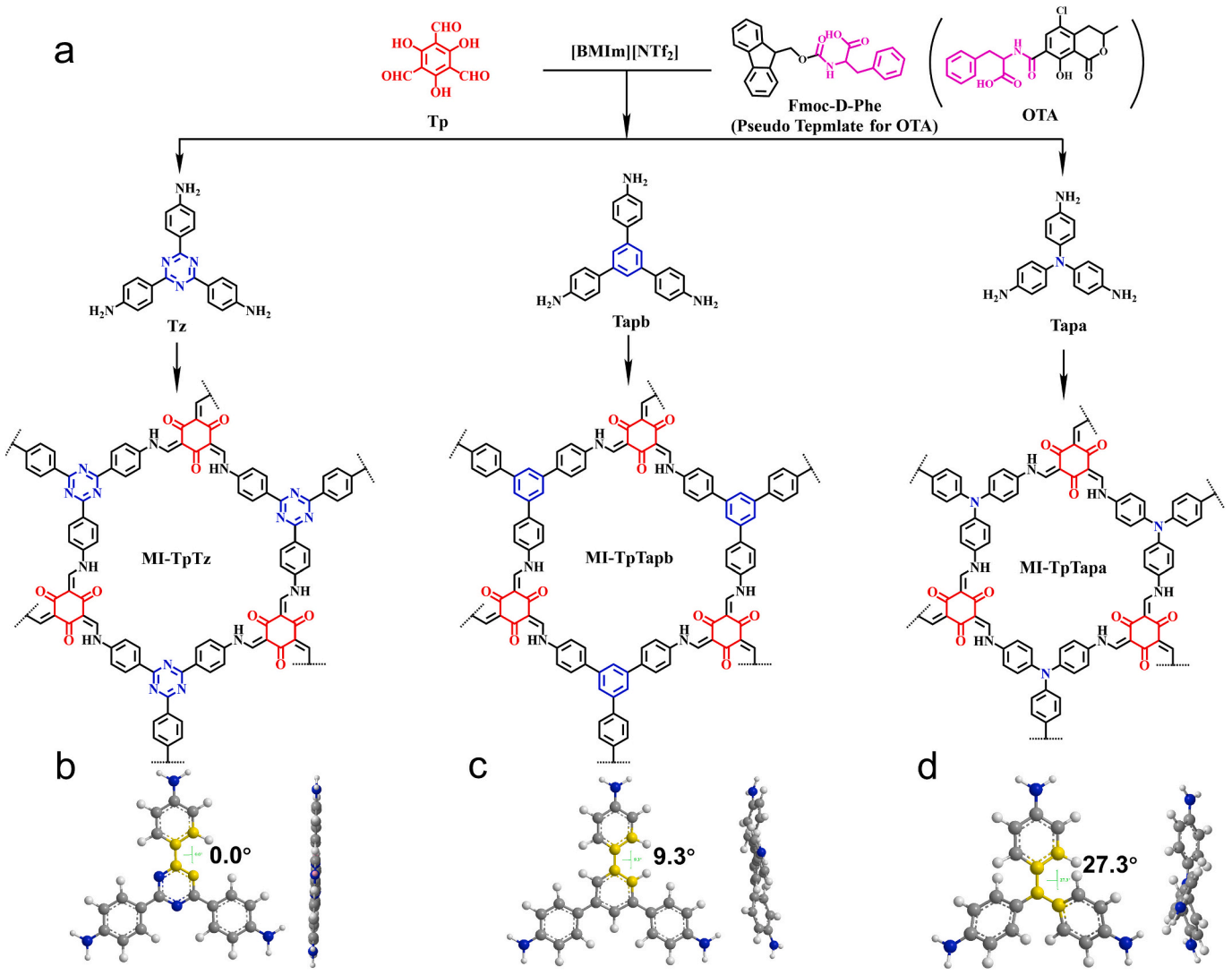

Fig. 1. (a) Scheme for the synthesis of MI-COFs via monomer planarity modulation strategy. The dihedral angle and side view after energy minimization of Tz (b), Tapb (c) and Tapa (d).

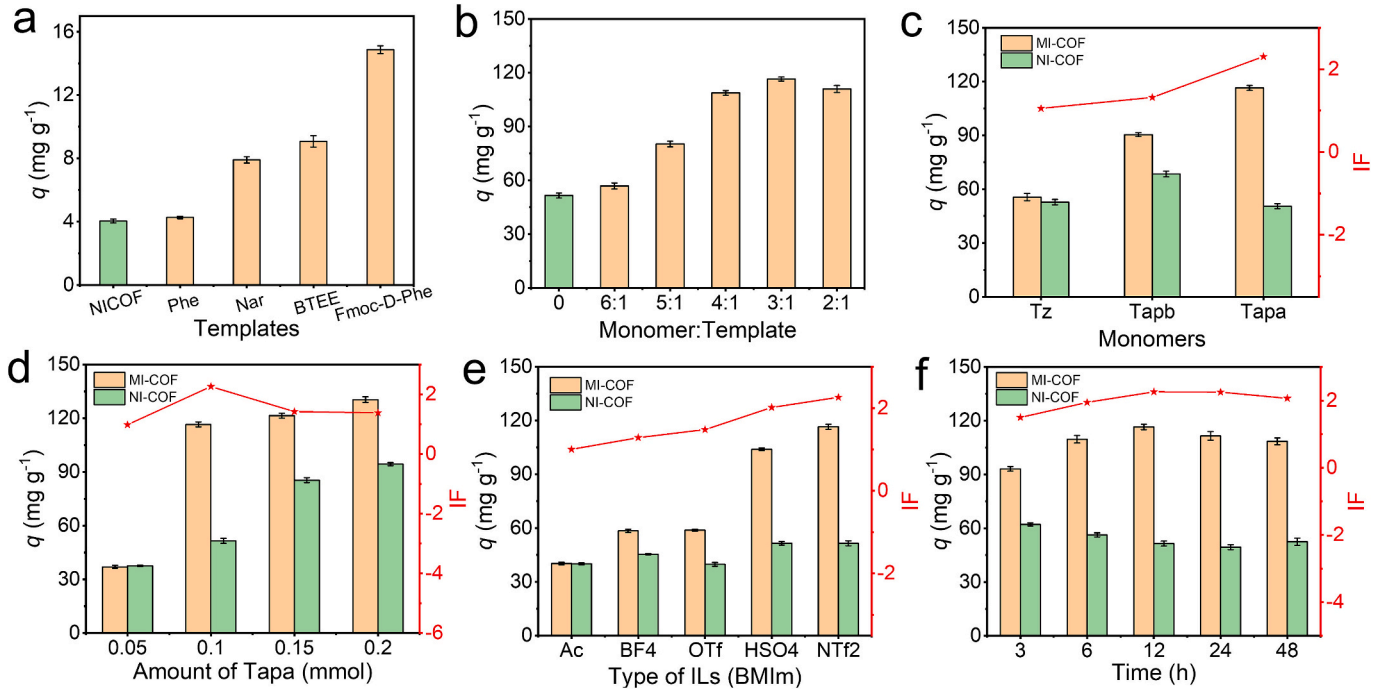

Fig. 2. Effect of synthetic conditions on the imprinting effect of MI-COF. (a) Pseudo template; (b) amount of template; (c) triamine modulator; (d) amount of Tapa; (e) type of ILs and (f) polymerization time.

imprinted cavities in MI-COFs in the presence of the template. Moreover, 0.1 mmol of Tapa gave the highest IF. Further increase of the amount of Tapa resulted in the decrease of IF value (Fig. 2d). Thus, 0.01 mmol of Tapa was selected for further experiments.

Solvents and catalysts are the key factors in the synthesis of MI-COFs. ILs were considered as green solvents and chosen as both solvent and catalyst for the synthesis of COFs (Guan et al., 2018; Qiu et al., 2020). Different [BMIm]-based ILs were used as both solvent and catalyst to investigate the effect on imprinting effect. MI-TpTapa synthesized in 200 μL of [BMIm][NTf_2] gave better imprinting effect (Fig. 2e and S3). The effect of polymerization time on the imprinting effect is shown in Fig. 2f. The value of IF increased with polymerization time, and reached the maximum at 12 h.

3.2. Characterization of MI-COFs and NI-COFs

The as-prepared MI-COFs and NI-COFs were characterized by Fourier transform-infrared (FT-IR) spectroscopy, powder X-ray diffraction (PXRD) analysis, scanning electron microscopy (SEM) and N_2 adsorption-desorption experiments. The disappearance of C═OH (2893 cm^{-1}) of Tp and N—H (3200–3500 cm^{-1}) of triamine monomers in conjunction with the appearance of obvious peaks at 1607–1623 cm^{-1} of C═O and 1278–1296 cm^{-1} of C − N confirms the ketone formation in the MI-COFs and NI-COFs (Fig. 3a) (Kandambeth et al., 2012). The dominant diffraction peaks at 5.74° in NI-TpTz, 5.69° in NI-TpTapb and 6.14° in NI-TpTapa identified the ordered structure, which is consistent with the simulated PXRD pattern of their AA stacking (Fig. 3b and S4). NI-TpTz with the highest planarity gave the best crystallinity due to the stronger interlay interaction (Da et al., 2020). Meanwhile, the dominant peaks in MI-TpTz, MI-TpTapb and MI-TpTapa were shifted to 5.64°, 5.59° and 5.89°, respectively, indicating the stretching of MI-COFs resulted from the presence of template. Moreover, MI-TpTapa exhibited the larger peak shift ($\Delta_{2\theta} = -0.25°$) than MI-TpTz ($\Delta_{2\theta} = -0.1°$) and MI-TpTapb ($\Delta_{2\theta} = -0.1°$).

MI-COFs gave lager Brunauer-Emmett-Teller (BET) surface areas than the corresponding NI-COFs. Among MI-COFs, MI-TpTapa gave the largest surface area of 706 $m^2\ g^{-1}$ (Fig. S5 − S6). The pore-size distributions of MI-COFs and NI-COFs were analyzed based on quenched solid density functional theory (QSDFT). For a certain triamine monomer, MI-COFs gave larger pore size the corresponding NI-COFs, indicating that the existence of template affected the pore size of MI-COFs (Ji et al., 2018). In addition, the difference of pore size between MI-COFs and NI-COFs decreased as the increase in the planarity of triamine monomers (Fig. 3c). MI-TpTapa showed more net stucture than of NI-TpTapa (Fig. 3d vs 3e). No significant difference was found in the SEM images of the other MI-COFs and NI-COFs (Fig. 3f−3i).

3.3. Adsorption study

The adsorption equilibrium experiments were performed in the initial Fmoc-D-Phe concentration range of 40–200 mg L^{-1} (Fig. 4a). The Langmuir model fitted better for MI-COFs and NI-COFs than the Freundlich model via both linear and non-linear fitting (Eq. S1 − S3, Fig. S7 and Table S1), indicating the adsorption of Fmoc-D-Phe onto MI-COFs and NI-COFs was monolayer with a limited adsorption site (Cheng et al., 2021). The theoretical maximum sorption capacities of NI-COFs decreased in the order of NI-TpTapb (194.8 mg g^{-1}) > NI-TpTz (154.5 mg g^{-1}) > NI-TpTapa (113.8 mg g^{-1}). The lowest binding energies between NI-COFs and Fmoc-D-Phe were calculated in the order of NI-TpTapb (− 7.5 kcal mol^{-1}) < NI-TpTapa (− 6.3 kcal mol^{-1}) < NI-TpTz (− 4.6 kcal mol^{-1}). NI-TpTz gave larger adsorption capacity than NI-TpTapa due to the exposure of more adsorption sites in high crystallinity NI-TpTz (Li, Yang, Qian, & Yan, 2023). The theoretical maximum adsorption capacities of MI-COFs decreased in the order of MI-TpTapa (471.4 mg g^{-1}) > MI-TpTapb (330.3 mg g^{-1}) > MI-TpTz (168.6 mg g^{-1}), and the values of IF were calculated to 4.1, 1.7 and 1.1, respectively, which is negatively correlated with their planarity. In other words, the lowest planarity of MI-TpTapa gave the best imprinting effect. The separation factors (R_L) and intensity factor $1/n$ of MI-COFs and NI-COFs were in the range of 0 to 1, indicating a favorable adsorption (Farrukh et al., 2013; Nayab et al., 2014). Distribution coefficient (K_d) was calculated to evaluate the affinity of sorbent to target. MI-TpTapa gave 4.8-fold K_d of NI-TpTapa (Table S1).

The adsorption kinetics was analyzed with the initial Fmoc-D-Phe

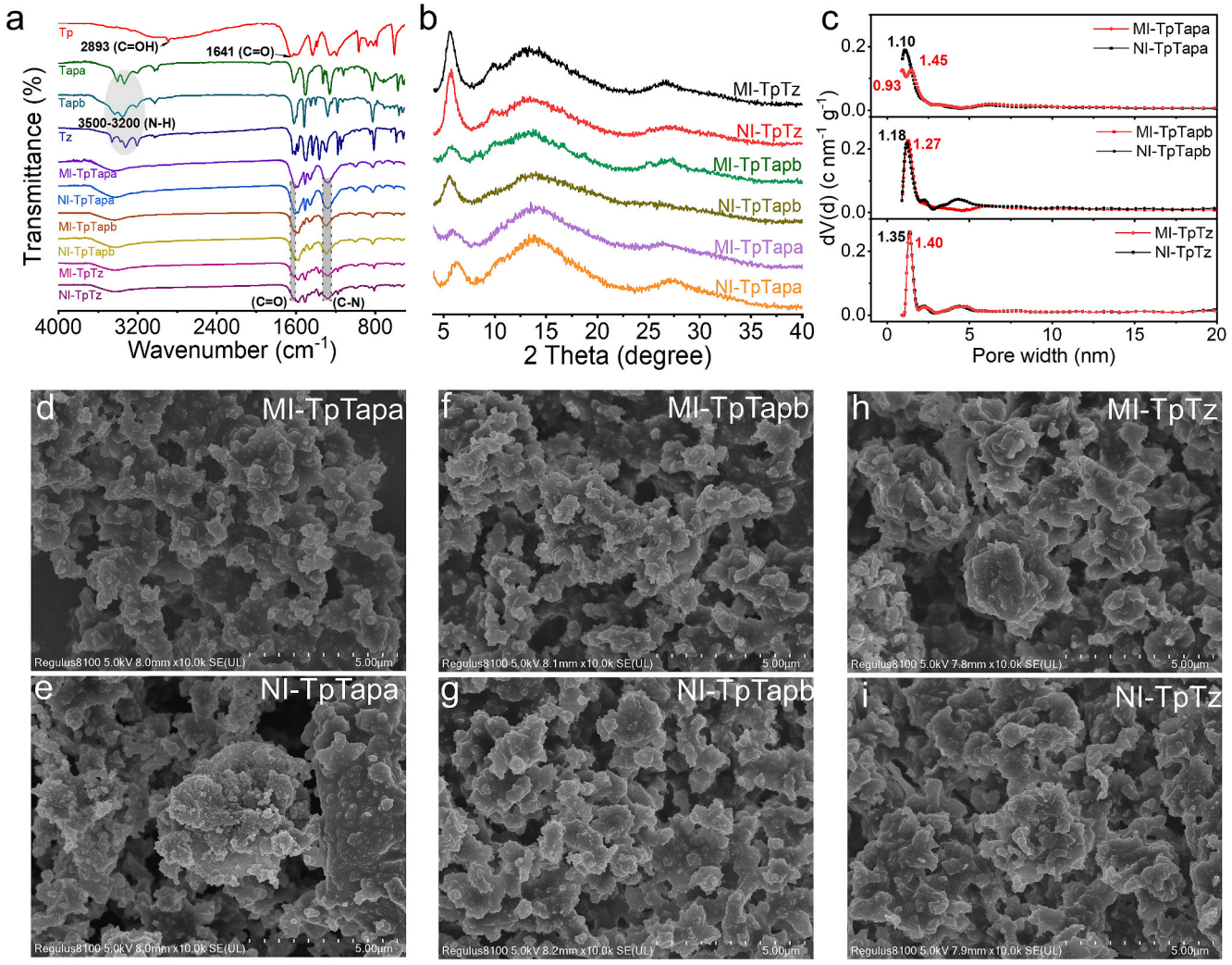

Fig. 3. (a) FT-IR spectra of Tp, triamine monomer, MI-COFs and NI-COFs. PXRD patterns (b), pore size distribution (c) and SEM images (d-i) of MI-COFs (d, f and h) and NI-COFs (e, g and i).

concentration of 20 mg L^{-1} (Fig. 4b and Table S2). MI-COFs showed faster kinetics for adsorption equilibrium (10 min) than NI-COFs (20 min), except from MI-TpTz and NI-TpTz (10 min for all). The pseudo-first-order model adsorption kinetic model was superior to the pseudo-second-order kinetic model via nonlinear fitting (Eq. S5 – S7, Table S2). However, the linear fitting gave the opposite results (Fig. S8). To better understand the adsorption processes, mix-order kinetic model was further stablished to analyze the pseudo-first-order and pseudo-second-order kinetic model simultaneously (Eq. S8, Fig. S9) (Zhuang, Chen, Liu, & Wang, 2020). The obtained rate constants of the pseudo-first-order and pseudo-second-order models (k_1' and k_2') indicate that the adsorption process included both pseudo-first-order and pseudo-second-order kinetics models (Guo & Wang, 2019). The contributions of the pseudo-first-order rate were larger than the pseudo-second-order rate in three NI-COFs and MI-TpTz. On the contrary, the pseudo-second-order rate was higher than the pseudo-first-order rate at the initial stage of adsorption process in MI-TpTapa and MI-TpTapb, indicating the imprinted sites contributed to the pseudo-second-order kinetics in adsorption process.

The adsorption of four mycotoxins (OTA, ZEN, AFB1 and DON) on MI-COFs and NI-COFs was studies to test the selectivity of MI-COFs to OTA (Fig. 4c). The K_d, selectivity coefficient (K) and relative selectivity coefficient (K') of MI-COFs and NI-COFs were calculated based on Eq. S4, S9 and S10 (Table S3) (Cui et al., 2020). MI-TpTapa and MI-TpTapb gave larger K_d values towards OTA than other three mycotoxins. Furthermore, the K' values of MI-TpTapa, MI-TpTapb and MI-TpTz for OTA towards other three mycotoxins were 3.77 – 3.87, 1.88 – 1.98 and 1.04 – 1.07, respectively, showing higher selectivity of MI-TpTapa to OTA.

The effect of pH on the adsorption capacity of MI-TpTapa for Fmoc-D-Phe was studied (Fig. S10). The pK_a of Fmoc-D-Phe is 3.77. The zeta potential reveals that the isoelectric point of MI-TpTapa was in the pH range of 5–6. The adsorption capacity is the largest at pH 4, where MI-TpTapa is positively charged while Fmoc-D-Phe is negatively charged. Electrostatic repulsion between MI-TpTapa and Fmoc-D-Phe existed in other pH, resulting in the lower adsorption capacity.

3.4. Interaction study

The effect of the planarity of monomers on the interlayer interaction in COFs was investigated. The calculated stacking energies of TpTz (– 143.9 kJ mol^{-1}), TpTapb (– 133.8 kJ mol^{-1}) and TpTapa (– 112.2 kJ mol^{-1}) increased as the planarity of monomers decreased (Fig. 5a). The more negative stacking energy in TpTz indicates the more stable system, which is consistent with previous studies (Da et al., 2020; Jiang et al., 2022). However, TpTapa with larger interlamellar spacing and weak interlayer interaction led to the easy formation of imprinted sites in the presence of pseudo templates. Fig. 5b shows the electrostatic potential (ESP) distribution of the OTA, Fmoc-D-Phe and MI-TpTapa. The N—H in

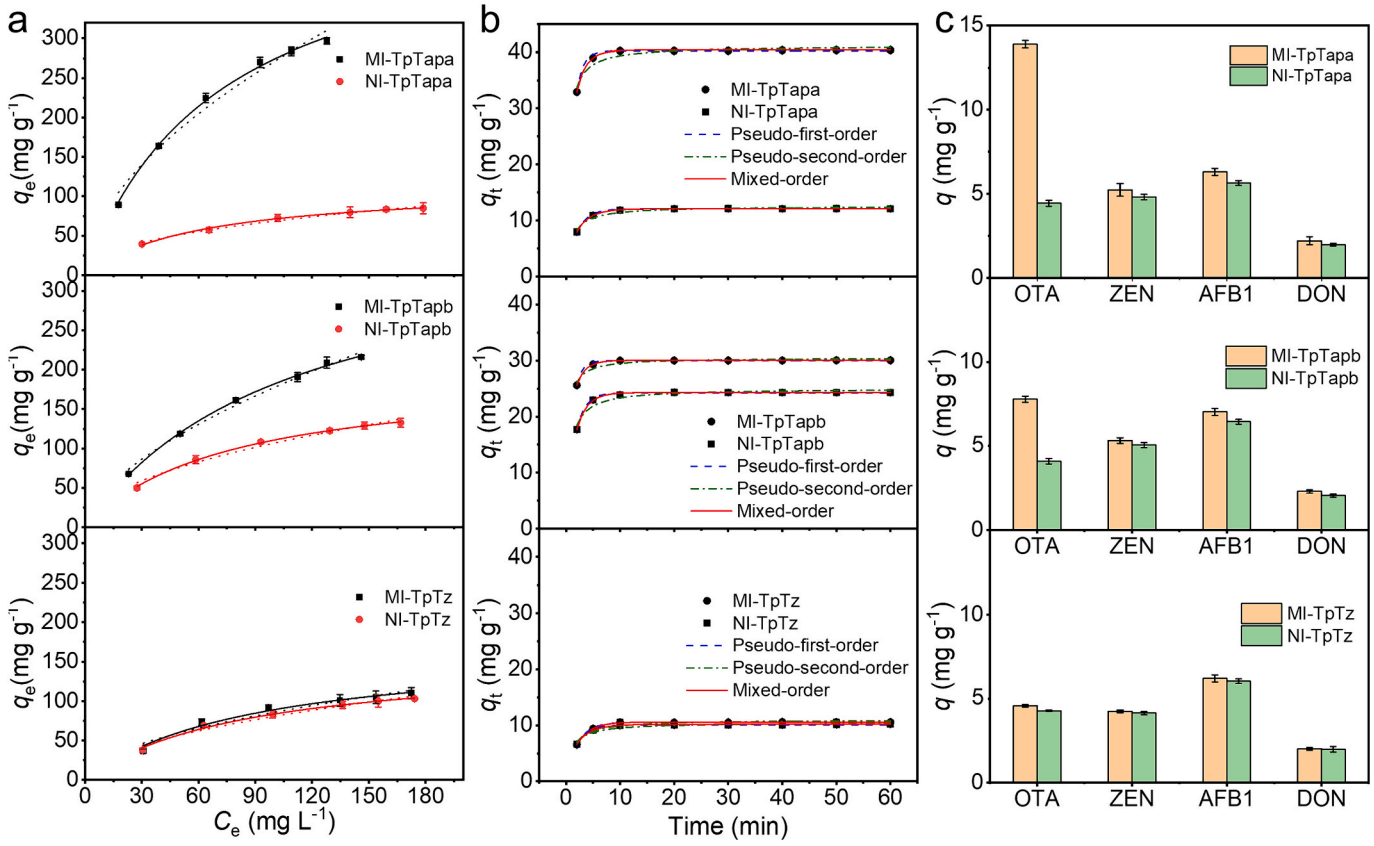

Fig. 4. (a) Adsorption isotherms of Fmoc-D-Phe (4 mL, 40–200 mg L^{-1}) on MI-COFs and NI-COFs (1 mg). The solid and dashed lines represent the fitting Langmuir and Freundlich models, respectively; (b) adsorption kinetics for Fmoc-D-Phe (4 mL, 20 mg L^{-1}) on MI-COF and NI-COF (1 mg); (c) adsorption selectivity of MI-COFs and NI-COFs (1 mg) towards OTA against ZEN, AFB1 and DON (4 mL, 10 mg L^{-1}).

OTA and Fmoc-D-Phe is the hydrogen bond donor site, meanwhile the C═O in the MI-TpTapa provides the hydrogen bond receptor site. This phenomenon further proves the hydrogen bond interaction of N-H…C=O.

The FT-IR spectra of MI-TpTapa after and before the adsorption of Fmoc-D-Phe and OTA are shown in Fig. S11. The peaks of aromatic C—H bending (823 cm^{-1}) and phenyl C═C stretching vibrations (1451 cm^{-1}) in MI-TpTapa shifted to 825 cm^{-1} and 1453 cm^{-1} after the adsorption of Fmoc-D-Phe and OTA, respectively, due to the π-π interaction between the adsorbate and MI-COF (Kumar et al., 2018; Xiong et al., 2019). Meanwhile, the C═O stretching of MI-TpTapa at 1607 cm^{-1} moved to 1609 and 1610 cm^{-1} after Fmoc-D-Phe and OTA loading, respectively, indicating the existence of hydrogen bond interaction (Xu, Zhu, Xia, & Wang, 2021).

The interaction was further verified by XPS (Fig. S12). The appearance of the new peaks associated to C—O in C 1 s and O 1 s demonstrated the adsorption of Fmoc-D-Phe and OTA on MI-TpTapa (Fig. 5c and d). The peaks of C 1 s for C═O in MI-TpTapa changed from 288.15 eV to 288.37 and 288.47 eV after the adsorption of Fmoc-D-Phe and OTA, respectively (Fig. 5c). The characteristic peaks of N 1 s for C—N in MI-TpTapa shifted from 400.12 eV to 400.31 and 400.29 eV after the adsorption of Fmoc-D-Phe and OTA, respectively (Fig. 5d). Meanwhile, the peak of O 1 s for C═O was also moved to higher binding energies after sorption (Fig. 5e), indicating that the C═O was concerned with the adsorption of Fmoc-D-Phe and OTA (Zhao et al., 2021). The high-resolution XPS spectra for original Fmoc-D-Phe also show the movement in the peaks of C—N and C═O (Fig. S13). The above results demonstrate the presence of hydrogen bonding (C=O…H-N) in MI-TpTapa with Fmoc-D-Phe and OTA, which is consistent with molecular docking results.

3.5. Optimization of DSPE

The conditions of DSPE including pH (3–9), adsorbent dosage (1–8 mg), extraction time (1–10 min), the content of FA (0%–70%) in the elution solvent ACN/FA, elution volume (0.5–3.0 mL) and elution time (1–10 min) were optimized with the concentration of 2 μg kg^{-1} OTA. The high OTA affinity of MI-TpTapa gave high recovery (above 96.5%) in the studied pH range of 4–9 (Fig. S14a). The pH range of 4–6 gave relatively higher recovery (above 98%). Therefore, pH 4 was selected for subsequent experiments. The recovery increased as the dosage of MI-TpTapa increased to 4 mg and then reached a platform (Fig. S14b), so 4 mg of MI-TpTapa was used in extraction. The recovery reached 98% with 2 min of extraction time, then leveled off (Fig. S14c). Hence, 2 min was adapted as extraction time. The optimization of elution solvent, volume and time showed the application of 1.0 mL of ACN/FA (4:6, *v*/v) for 2 min gave the best elution efficiency (Fig. S14d–f).

3.6. Analytical performance

The calibration curves with the linear range of 0.1–1000 μg kg^{-1} were obtained by using OTA-free alcohol samples standard addition method under the optimized DSPE conditions (Fig. S15), and the coefficients of determination (R^2) ranged from 0.9994 to 0.9999. Matrix effects were calculated in the range of 0.9716 to 0.9807 (Table S4). Moreover, the sensitivity of OTA in sample matrix and that in standard solution were evaluated by *t*-test ($1.30 < P < 1.58$), showing no significant difference. These results illustrate the negligible matrix effect in the developed MI-TpTapa-based DSPE method, meaning that the standard curve calibration can be used for the quantitation of OTA in real samples. The limits of detection (LOD, S/N = 3) and quantification (LOQ, S/*N* = 10) were 0.023 and 0.078 μg kg^{-1}, respectively, which are

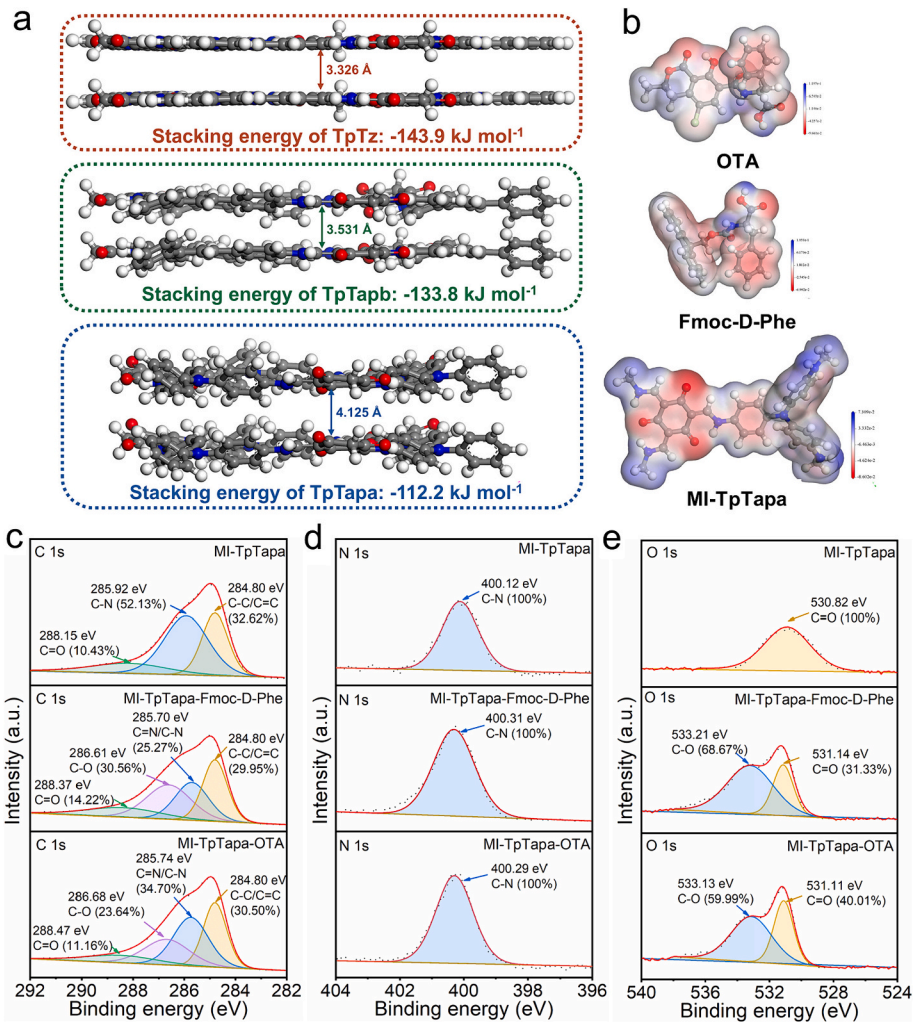

Fig. 5. (a) Stacking energies of studied COFs. (b) Electrostatic potential distribution mapping of OTA, Fmoc-D-Phe and MI-TpTapa. High-resolution XPS spectra of C 1 s (c), N 1 s (d) and O 1 s (e) for MI-TpTapa, MI-TpTapa-Fmoc-D-Phe and MI-TpTapa-OTA (dashed lines and red lines represent raw curves and fitting curves, respectively). (For interpretation of the references to colour in this figure legend, the reader is referred to the web version of this article.)

considerably lower than the MRL (2 μg kg^{-1}) for OTA in alcohol. The relative standard deviation (RSD, $n = 6$) of intra and inter day was <3.2% (Table S5). The developed method was compared with other reported methods (Table S6), showing the lower detection limit, higher accuracy, higher precision and wider linear range than other reported methods.

The selective extraction performance of MI-TpTapa for OTA was studied by adding other mycotoxins (ZEN, AFB1 and DON) into the extraction process. The recoveries of OTA were still over 97% in presence of other mycotoxins (Fig. S16) due to the high selectivity of MI-TpTapa for OTA. Furthermore, the recycling times of the MI-TpTapa was also investigated (Fig. S17). After five cycles of uses, the MI-TpTapa still gave over 94% of recovery for OTA. No obvious change was observed in the FI-IR spectra and PXRD pattern (Fig. S18) of the fresh and regenerated MI-TpTapa, showing a good reusability.

3.7. Application to real samples

Alcohol samples (beer, red wine and soju) were analyzed by the developed DSPE method in combination with HPLC-FLD. The absolute recoveries for the spiked OTA in the concentration range of 0–10 μg kg^{-1} in these samples ranged from 91.4% to 97.6% (Table 1), and a contaminated beer sample was found (concentration of OTA was 0.126 ± 0.008 μg kg^{-1}, Fig. S19).

4. Conclusion

We have proposed a monomer planarity modulation strategy for room-temperature constructing of MI-COFs for selective extraction of OTA. We have highlighted that the non-planar MI-COFs with weak interlayer interaction led to the easy formation of imprinted sites in the presence of pseudo templates. The proposed preparation method allows the room-temperature synthesis of highly selective MI-COFs in an open environment. The as-prepared MI-TpTapa gave higher selectivity for OTA than other more planar MI-COFs. The use of the prepared MI-TpTapa as adsorbent for the DSPE of OTA before HPLC determination allows matrix effect-free determination of OTA in real samples. The developed method shows shorter extraction time, lower detection limit, higher accuracy, higher precision and wider linear range than other reported methods. We believe that combining the interlayer interaction modulation strategy with rational selecting pseudo template will open a new train of thoughts to construct MI-COFs for selective extraction of hazardous compounds.

CRediT authorship contribution statement

Hao-Ze Li: Writing – original draft, Validation, Investigation, Data curation, Conceptualization. **Hai-Long Qian:** Validation. **Shu-Ting Xu:** Validation. **Cheng Yang:** Validation. **Xiu-Ping Yan:** Writing – review &

Table 1
Analytical results for real samples using the developed method.

Sample	Spiked OTA (μg kg^{-1})	Concentration determined (μg kg^{-1}, mean ± s, n = 6)	Absolute recovery (%, mean ± s, n = 6)
Beer 1	0	0.126 ± 0.008	–
	1	1.094 ± 0.019	96.8 ± 1.9
	5	4.844 ± 0.017	94.4 ± 0.3
	10	9.434 ± 0.037	93.1 ± 0.4
Beer 2	0	ND[a]	–
	1	0.961 ± 0.019	96.1 ± 1.9
	5	4.700 ± 0.107	94.0 ± 2.1
	10	9.432 ± 0.095	94.3 ± 0.9
Red wine 1	0	ND[a]	–
	1	0.914 ± 0.021	91.4 ± 2.1
	5	4.768 ± 0.152	95.4 ± 3.0
	10	9.336 ± 0.268	93.4 ± 2.7
Red wine 2	0	<LOQ	–
	1	0.926 ± 0.012	92.6 ± 1.2
	5	4.882 ± 0.033	97.6 ± 0.7
	10	9.453 ± 0.116	94.5 ± 1.2
Soju 1	0	ND[a]	–
	1	0.947 ± 0.011	94.7 ± 1.1
	5	4.603 ± 0.126	92.0 ± 2.5
	10	9.624 ± 0.155	96.2 ± 1.6
Soju 2	0	ND[a]	–
	1	0.936 ± 0.008	93.6 ± 0.8
	5	4.744 ± 0.063	94.9 ± 1.3
	10	9.545 ± 0.112	95.4 ± 1.1

[a] ND, Not detected.

editing, Supervision, Project administration, Funding acquisition, Conceptualization.

Declaration of competing interest

The authors declare that they have no known competing financial interests or personal relationships that could have appeared to influence the work reported in this paper.

Data availability

Data will be made available on request.

Acknowledgements

This work was supported by the National Natural Science Foundation of China (22176073) and the Program of “Collaborative Innovation Center of Food Safety and Quality Control in Jiangsu Province”.

Appendix A. Supplementary data

Supplementary data to this article can be found online at https://doi.org/10.1016/j.foodchem.2024.139427.

References

Bui-Klimke, T. R., & Wu, F. (2015). Ochratoxin A and human health risk: A review of the evidence. *Critical Reviews in Food Science and Nutrition, 55*(13), 1860–1869. https://doi.org/10.1080/10408398.2012.724480

Chen, L., Wu, Q., Gao, J., Li, H., Dong, S., Shi, X., & Zhao, L. (2019). Applications of covalent organic frameworks in analytical chemistry. *TrAC Trends in Analytical Chemistry, 113*, 182–193. https://doi.org/10.1016/j.trac.2019.01.016

Cheng, G., Li, X., Li, X., Chen, J., Liu, Y., Zhao, G., & Zhu, G. (2021). Surface imprinted polymer on a metal-organic framework for rapid and highly selective adsorption of sulfamethoxazole in environmental samples. *Journal of Hazardous Materials, 423*(Pt A), Article 127087. https://doi.org/10.1016/j.jhazmat.2021.127087

Cui, Y., Kang, W., Qin, L., Ma, J., Liu, X., & Yang, Y. (2020). Magnetic surface molecularly imprinted polymer for selective adsorption of quinoline from coking wastewater. *Chemical Engineering Journal, 397*(1), Article 125480. https://doi.org/10.1016/j.cej.2020.125480

Cui, Y., Ma, H., Liu, D., Li, M., Hao, R., Li, J., & Jiang, Y. (2020). Graphene oxide adsorbent-based dispersive solid phase extraction coupled with multi-pretreatment clean-up for analysis of trace Ochratoxin A in chicken liver. *Chromatographia, 83*(10), 1307–1314. https://doi.org/10.1007/s10337-020-03942-8

Da, H.-J., Yang, C.-X., Qian, H.-L., & Yan, X.-P. (2020). A knot-linker planarity control strategy for constructing highly crystalline cationic covalent organic frameworks: Decoding the effect of crystallinity on adsorption performance. *Journal of Materials Chemistry A, 8*(25), 12657–12664. https://doi.org/10.1039/d0ta01037e

Du, L.-J., Chu, C., Warner, E., Wang, Q.-Y., Hu, Y.-H., Chai, K.-J., … Zhang, Q.-D. (2018). Rapid microwave-assisted dispersive micro-solid phase extraction of mycotoxins in food using zirconia nanoparticles. *Journal of Chromatography A, 1561*, 1–12. https://doi.org/10.1016/j.chroma.2018.05.031

Elik, A., Ablak, Ö., Haq, H. U., Boczkaj, G., & Altunay, N. (2023). Combination of homogeneous liquid–liquid extraction and vortex assisted dispersive liquid–liquid microextraction for the extraction and analysis of ochratoxin A in dried fruit samples: Central composite design optimization. *Journal of Food Composition and Analysis, 124*, Article 105656. https://doi.org/10.1016/j.jfca.2023.105656

Fadlalla, M. H., Ling, S., Wang, R., Li, X., Yuan, J., Xiao, S., … Wang, S. (2020). Development of ELISA and Lateral flow immunoassays for Ochratoxins (OTA and OTB) detection based on monoclonal antibody. *Frontiers in Cellular and Infection Microbiology, 10*. https://doi.org/10.3389/fcimb.2020.00080

Farrukh, A., Akram, A., Ghaffar, A., Hanif, S., Hamid, A., Duran, H., & Yameen, B. (2013). Design of polymer-brush-grafted magnetic nanoparticles for highly efficient water remediation. *ACS Applied Materials & Interfaces, 5*(9), 3784–3793. https://doi.org/10.1021/am400427n

Guan, X., Ma, Y., Li, H., Yusran, Y., Xue, M., Fang, Q., … Qiu, S. (2018). Fast, ambient temperature and pressure Ionothermal synthesis of three-dimensional covalent organic frameworks. *Journal of the American Chemical Society, 140*(13), 4494–4498. https://doi.org/10.1021/jacs.8b01320

Guo, X., & Wang, J. (2019). A general kinetic model for adsorption: Theoretical analysis and modeling. *Journal of Molecular Liquids, 288*, Article 111100. https://doi.org/10.1016/j.molliq.2019.111100

Halder, A., Kandambeth, S., Biswal, B. P., Kaur, G., Roy, N. C., Addicoat, M., … Banerjee, R. (2016). Decoding the morphological diversity in two dimensional crystalline porous polymers by Core planarity modulation. *Angewandte Chemie International Edition, 55*(27), 7806–7810. https://doi.org/10.1002/anie.201600087

Han, S., Leng, Q., Teng, F., Ding, Y., & Yao, A. (2022). Preparation of mesh covalent organic framework Tppa-2-based adsorption enhanced magnetic molecularly imprinted composite for selective extraction of tetracycline residues from animal-derived foods. *Food Chemistry, 384*, Article 132601. https://doi.org/10.1016/j.foodchem.2022.132601

Huertas-Pérez, J. F., Arroyo-Manzanares, N., García-Campaña, A. M., & Gámiz-Gracia, L. (2017). Solid phase extraction as sample treatment for the determination of Ochratoxin A in foods: A review. *Critical Reviews in Food Science and Nutrition, 57*(16), 3405–3420. https://doi.org/10.1080/10408398.2015.1126548

Jagirani, M. S., Gumus, Z. P., & Soylak, M. (2023). Covalent organic frameworks, a renewable and emergent source for the separation and pre-concentration of the traces of targeted species. *Microchemical Journal, 191*, Article 108820. https://doi.org/10.1016/j.microc.2023.108820

Jagirani, M. S., & Soylak, M. (2020). A review: Recent advances in solid phase microextraction of toxic pollutants using nanotechnology scenario. *Microchemical Journal, 159*, Article 105436. https://doi.org/10.1016/j.microc.2020.105436

Ji, W., Sun, R., Geng, Y., Liu, W., & Wang, X. (2018). Rapid, low temperature synthesis of molecularly imprinted covalent organic frameworks for the highly selective extraction of cyano pyrethroids from plant samples. *Analytica Chimica Acta, 1001*, 179–188. https://doi.org/10.1016/j.aca.2017.12.001

Jiang, G., Zou, W., Ou, Z., Zhang, L., Zhang, W., Wang, X., … Du, L. (2022). Tuning the interlayer interactions of 2D covalent organic frameworks enables an Ultrastable platform for anhydrous proton transport. *Angewandte Chemie International Edition, 61*(35), Article e202208086. https://doi.org/10.1002/anie.202208086

Kabak, B. (2012). Determination of aflatoxins and ochratoxin A in retail cereal products from Turkey by high performance liquid chromatography with fluorescence detection. *Food Control, 28*(1), 1–6. https://doi.org/10.1016/j.foodcont.2012.04.043

Kandambeth, S., Mallick, A., Lukose, B., Mane, M. V., Heine, T., & Banerjee, R. (2012). Construction of crystalline 2D covalent organic frameworks with remarkable chemical (acid/base) stability via a combined reversible and irreversible route. *Journal of the American Chemical Society, 134*(48), 19524–19527. https://doi.org/10.1021/ja308278w

Kumar, A. G., Singh, A., Komber, H., Voit, B., Tiwari, B. R., Noori, M. T., … Banerjee, S. (2018). Novel sulfonated co-poly(ether imide)s containing Trifluoromethyl, Fluorenyl and hydroxyl groups for enhanced proton exchange membrane properties: Application in microbial fuel cell. *ACS Applied Materials & Interfaces, 10*(17), 14803–14817. https://doi.org/10.1021/acsami.8b03452

Li, C.-Y., Lv, S.-W., Yang, L., Wang, J., Liu, J.-M., & Wang, S. (2022). Facile preparation of uniform-sized covalent organic framework nanoflowers as versatile sample-pretreatment platforms for sensitive and specific determination of hazardous substances. *Journal of Hazardous Materials, 438*, Article 129566. https://doi.org/10.1016/j.jhazmat.2022.129566

Li, H.-Z., Yang, C., Qian, H.-L., & Yan, X.-P. (2023). Room-temperature synthesis of ionic covalent organic frameworks for efficient removal of diclofenac sodium from aqueous solution. *Separation and Purification Technology, 306*, Article 122704. https://doi.org/10.1016/j.seppur.2022.122704

Li, J., Xu, X., Guo, W., Zhang, Y., Feng, X., & Zhang, F. (2022). Synthesis of a magnetic covalent organic framework as sorbents for solid-phase extraction of aflatoxins in food prior to quantification by liquid chromatography-mass spectrometry. *Food Chemistry, 387*, Article 132821. https://doi.org/10.1016/j.foodchem.2022.132821

Li, W., Chen, N., Zhu, Y., Shou, D., Zhi, M., & Zeng, X. (2019). A nanocomposite consisting of an amorphous seed and a molecularly imprinted covalent organic framework shell for extraction and HPLC determination of nonsteroidal anti-inflammatory drugs. *Microchimica Acta, 186*(2), 76. https://doi.org/10.1007/s00604-018-3187-6

Li, X., Ma, W., Ma, Z., Zhang, Q., & Li, H. (2021a). The occurrence and contamination level of Ochratoxin a in plant and animal-derived food commodities. *Molecules, 26*(22), 6928. https://www.mdpi.com/1420-3049/26/22/6928.

Li, X., Ma, W., Ma, Z., Zhang, Q., & Li, H. (2021b). Recent progress in determination of ochratoxin a in foods by chromatographic and mass spectrometry methods. *Critical Reviews in Food Science and Nutrition, 62*(20), 5444–5461. https://doi.org/10.1080/10408398.2021.1885340

Liu, R., Tan, K. T., Gong, Y., Chen, Y., Li, Z., Xie, S., … Jiang, D. (2021). Covalent organic frameworks: An ideal platform for designing ordered materials and advanced applications. *Chemical Society Reviews, 50*(1), 120–242. https://doi.org/10.1039/d0cs00620c

Lohse, M. S., & Bein, T. (2018). Covalent organic frameworks: Structures, synthesis, and applications. *Advanced Functional Materials, 28*(33), 1705553. https://doi.org/10.1002/adfm.201705553

Ma, W., Zheng, Q., He, Y., Li, G., Guo, W., Lin, Z., & Zhang, L. (2019). Size-controllable synthesis of uniform spherical covalent organic frameworks at room temperature for highly efficient and selective enrichment of hydrophobic peptides. *Journal of the American Chemical Society, 141*(45), 18271–18277. https://doi.org/10.1021/jacs.9b09189

Martinez-Abadia, M., & Mateo-Alonso, A. (2020). Structural approaches to control interlayer interactions in 2D covalent organic frameworks. *Advanced Materials, 32*(40), Article e2002366. https://doi.org/10.1002/adma.202002366

Meira, D. I., Barbosa, A. I., Borges, J., Reis, R. L., Correlo, V. M., & Vaz, F. (2023). Recent advances in nanomaterial-based optical biosensors for food safety applications: Ochratoxin-A detection, as case study. *Critical Reviews in Food Science and Nutrition*, 1–43. https://doi.org/10.1080/10408398.2023.2168248

Mohebbi, A., Nemati, M., Farajzadeh, M. A., Afshar Mogaddam, M. R., & Lotfipour, F. (2022). High performance liquid chromatography-tandem mass spectrometry determination of patulin and ochratoxin a in commercial fruit juices after their extraction with a green synthesized metal organic framework-based dispersive micro solid phase extraction procedure. *Microchemical Journal, 179*, Article 107558. https://doi.org/10.1016/j.microc.2022.107558

Nayab, S., Farrukh, A., Oluz, Z., Tuncel, E., Tariq, S. R., ur Rahman, H., … Yameen, B. (2014). Design and fabrication of branched polyamine functionalized mesoporous silica: An efficient absorbent for water remediation. *ACS Applied Materials & Interfaces, 6*(6), 4408–4417. https://doi.org/10.1021/am500123k

Pittet, A., & Royer, D. (2002). Rapid, low cost thin-layer chromatographic screening method for the detection of Ochratoxin A in green coffee at a control level of 10 μg/kg. *Journal of Agricultural and Food Chemistry, 50*(2), 243–247. https://doi.org/10.1021/jf010867w

Qiu, J., Wang, H., Zhao, Y., Guan, P., Li, Z., Zhang, H., … Wang, J. (2020). Hierarchically porous covalent organic frameworks assembled in ionic liquids for highly effective catalysis of C–C coupling reactions. *Green Chemistry, 22*(8), 2605–2612. https://doi.org/10.1039/d0gc00223b

Samuel, M. S., Jeyaram, K., Datta, S., Chandrasekar, N., Balaji, R., & Selvarajan, E. (2021). Detection, contamination, toxicity, and prevention methods of Ochratoxins: An update review. *Journal of Agricultural and Food Chemistry, 69*(46), 13974–13989. https://doi.org/10.1021/acs.jafc.1c05994

Su, B., Zhang, Z., Sun, Z., Tang, Z., Xie, X., Chen, Q., … Hammock, B. D. (2022). Fluonanobody-based nanosensor via fluorescence resonance energy transfer for ultrasensitive detection of ochratoxin A. *Journal of Hazardous Materials, 422*, Article 126838. https://doi.org/10.1016/j.jhazmat.2021.126838

Vyas, V. S., Haase, F., Stegbauer, L., Savasci, G., Podjaski, F., Ochsenfeld, C., & Lotsch, B. V. (2015). A tunable azine covalent organic framework platform for visible light-induced hydrogen generation. *Nature Communications, 6*(1), 8508. https://doi.org/10.1038/ncomms9508

Wei, D., Pan, A., Zhang, C., Guo, M., Lou, C., Zhang, J., … Wang, X. (2023). Fast extraction of aflatoxins, ochratoxins and enniatins from maize with magnetic covalent organic framework prior to HPLC-MS/MS detection. *Food Chemistry, 404*, Article 134464. https://doi.org/10.1016/j.foodchem.2022.134464

Xin, J., Wang, X., Li, N., Liu, L., Lian, Y., Wang, M., & Zhao, R. S. (2020). Recent applications of covalent organic frameworks and their multifunctional composites for food contaminant analysis. *Food Chemistry, 330*, Article 127255. https://doi.org/10.1016/j.foodchem.2020.127255

Xiong, T., Yuan, X., Wang, H., Wu, Z., Jiang, L., Leng, L., … Zeng, G. (2019). Highly efficient removal of diclofenac sodium from medical wastewater by Mg/Al layered double hydroxide-poly(m-phenylenediamine) composite. *Chemical Engineering Journal, 366*, 83–91. https://doi.org/10.1016/j.cej.2019.02.069

Xu, H., Zhu, S., Xia, M., & Wang, F. (2021). Rapid and efficient removal of diclofenac sodium from aqueous solution via ternary core-shell CS@PANI@LDH composite: Experimental and adsorption mechanism study. *Journal of Hazardous Materials, 402*, Article 123815. https://doi.org/10.1016/j.jhazmat.2020.123815

Zhang, M., Zhang, S., Guo, X., Xun, Z., Wang, L., Liu, Y., … Peng, X. (2024). Fast, portable, selective, and ratiometric determination of ochratoxin A (OTA) by a fluorescent supramolecular sensor. *Journal of Hazardous Materials, 465*, Article 133104. https://doi.org/10.1016/j.jhazmat.2023.133104

Zhang, Y., Li, G., Wu, D., Li, X., Yu, Y., Luo, P., … Wu, Y. (2019). Recent advances in emerging nanomaterials based food sample pretreatment methods for food safety screening. *TrAC Trends in Analytical Chemistry, 121*, Article 115669. https://doi.org/10.1016/j.trac.2019.115669

Zhao, L., Lin, X., Duan, N., Mahmood Khan, I., Wang, Z., & Wu, S. (2023). A sensitive fluorescent assay based on gold-nanoclusters coated on molecularly imprinted covalent organic frameworks and its application in malachite green detection. *Food Chemistry, 410*, Article 135425. https://doi.org/10.1016/j.foodchem.2023.135425

Zhao, Q., Zhang, H., Zhao, H., Liu, J., Liu, J., Chen, Z., … Yang, X. (2020). Strategy of fusion covalent organic frameworks and molecularly imprinted polymers: A surprising effect in recognition and loading of Cyanidin-3-O-glucoside. *ACS Applied Materials & Interfaces, 12*(7), 8751–8760. https://doi.org/10.1021/acsami.9b21460

Zhao, R., Zheng, H., Zhong, Z., Zhao, C., Sun, Y., Huang, Y., & Zheng, X. (2021). Efficient removal of diclofenac from surface water by the functionalized multilayer magnetic adsorbent: Kinetics and mechanism. *Science of the Total Environment, 760*, Article 144307. https://doi.org/10.1016/j.scitotenv.2020.144307

Zhuang, S., Chen, R., Liu, Y., & Wang, J. (2020). Magnetic COFs for the adsorptive removal of diclofenac and sulfamethazine from aqueous solution: Adsorption kinetics, isotherms study and DFT calculation. *Journal of Hazardous Materials, 385*, Article 121596. https://doi.org/10.1016/j.jhazmat.2019.121596